DEFORMATION BEHAVIOR OF STEELS IN MUSHY STATE

A. A. Tseng
Department of Mechanical and Aerospace Engineering
Arizona State University
Tempe, Arizona 85287-6106 USA

J. Horský, M. Raudenský, and P. Kotrbácek
Fluid Flow and Heat Transfer Laboratory
Technical University of Brno
Brno, Czech Republic

Abstract

Processing metals in a semisolid or mushy state has emerged as a vital commercial process to produce metal and metal-matrix composite components. The understanding of the basic deformation behavior of materials in the mushy state is critical for better control of various semisolid processes. The aim of the present study is to quantify the flow stress of mushy-state steels under uniaxial deformation conditions. A hot compression tester has been developed to provide the high temperature setting required for testing mushy-state steels. An analytical scheme, which only requires measuring the dimensions of the final solidified specimen, has been developed to eliminate the barrelling effects occurring in compression test. The temperature of specimens has been carefully controlled to correlate the solid phase content. It has been found that the flow stress of steels in mushy states was highly dependent on the solid phase percentage. The relaxation of steel and stress reduction at mushy states were also discussed.

Introduction

Increasing attention is being given to net shape processing of metals at semisolid or mushy states (Flemings, 1991; Kiuchi, 1989). The semisolid or mushy-state process permits molten metals to partially solidify before shape-making operations. Among many benefits, it reduces the force requirement for the forging processes because of the lower flow stresses involved, or increases die life in die casting operations due to the lower temperature associated.

To understand the mushy-state processing behavior of any metals, it is essential to have the basic data, especially the flow stress and strain relationship. A great amount of work has been done in studying the semisolid structure and its rheological properties as well as the forming methodology. Most of work has been focused on the determination of material characteristics of relatively low-melting temperature materials, including aluminum, magnesium, tin, lead and their composites (Flemings, 1991; Kiuchi, 1989; Kattamis and Piccone, 1991; Kiuchi and Sugizama, 1992; Kumar, Martin, and Brown, 1993; Worster, 1997). Because of the high-melting temperatures and other related measurement difficulties, there is relatively a small amount of experimental data available on steels.

As a result, the purpose of the present study is to provide the basic deformation data for steel under mushy states. The flow stress of mushy-state steels under uniaxial conditions will be evaluated. A hot compression test is developed to generate the flow stress data. An analytical scheme will be used to eliminate the barrelling effects inherited in the compression test. Semisolid specimens were evaluated at various solid phase content. The changes in the percentage of solid phases are followed by changes in steel structures and rheology, which results in the change of the forming behavior. The correlation between the temperature and the percentage of the solid phase will be used to define the characteristics of the mushy state.

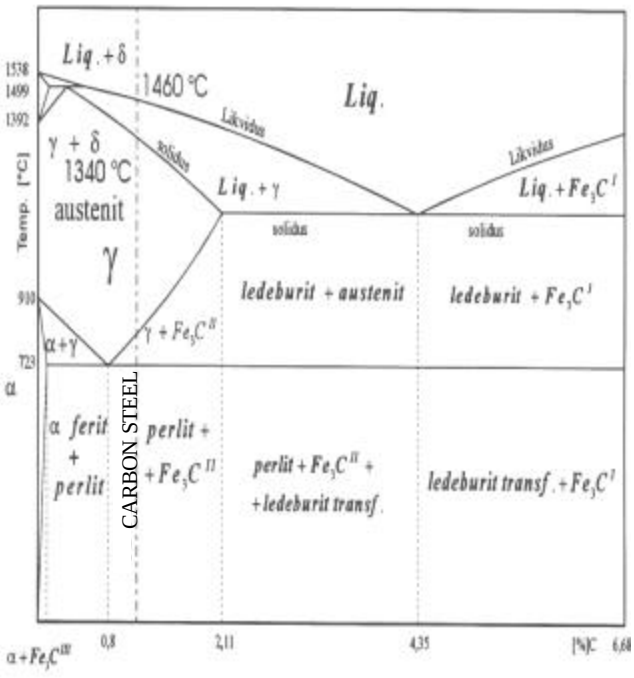

Figure 1. Iron-Carbon Metastable Phase Diagram

Material And Microstructures

A high-carbon tool steel was selected for the present deformation study. Its composition is shown in Table I. Because of its low content of additions, the equilibrium binary phase diagram of Fe-C can be used to define the solidus and liquidus temperatures as well as the percentage contents of the liquid phase.

Table I Chemical Composition of Steel Sample

ELEMENT	C [%]	Mn [%]	Si [%]
QUANTITY	0.95 – 1.10	0.20 - 0.35	0.30

Based on the Fe-C phase diagram shown in Fig. 1, the solidus temperature for the steel tested can be found to be approximately

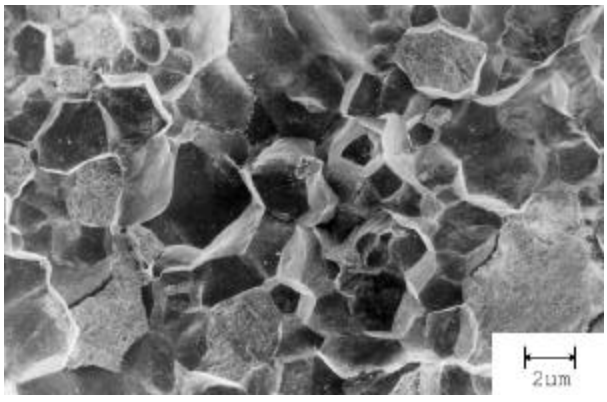

Figure 2. SEM Image of Quenched Sample

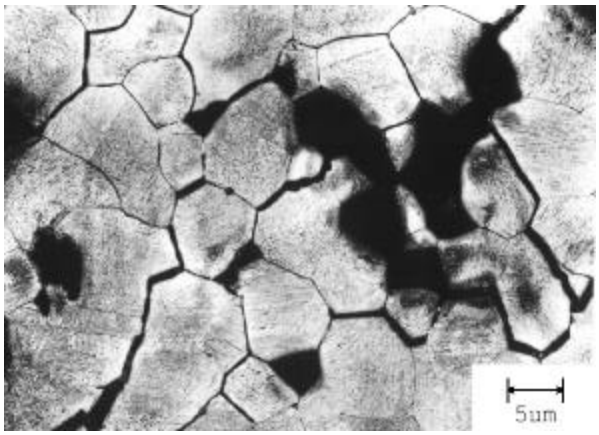

Figure 3. Optical Micrograph for Quenched Sample

1346 °C, and the liquidus temperature 1465 °C (Boyer and Gall, 1985). These temperatures are consistent with the measurement data obtained by a separate test. The difference between the liquidus and solidus temperatures is 119 °C and the well-known lever rule is used to estimate the contents of the solid and liquid phases by providing the testing temperature.

The microstructures of the selected material are studied. Material samples are first heated to a specific temperature within the mushy state, and then are quenched to the room temperature in which the microstructure and percentage of solid phase at the instant of quenching can be preserved. The quenched samples are examined with both optical and scanning electron microscopes. Examination by a scanning electron microscope, Fig. 2 depicts the intercrystalline fracture after heating the steel sample to a temperature of 1430 °C, having visible melting down of grain boundaries prior to quenching. Figure 3 shows the corresponding optical micrograph for a sample exposed to 1430 °C for one hour before quenching.

Apparatus And Testing

The apparatus used for the compression test has been specifically designed to accommodate the high temperatures required to melt steels. As shown in Fig. 4, it consists of an Instron load frame equipped with a position measuring device and a dynamometer with a range of up to 2 kN. A furnace specially designed to melt steels is situated within the load frame. The furnace is heated by two resistive heating elements placed at opposite ends of the furnace enclosure. Two thermocouples are placed inside the furnace; one is close to the material sample to ensure that the preset temperature is achieved. Temperatures monitored from either location have been consistent with each other. A microcomputer-based data acquisition system collects information from the dynamometer and records positions while the experiment is performed. The schematic diagram showing the major components of the apparatus is depicted in Fig. 5.

The steel sample is placed between two corundum fine-grained ceramic discs with a smoothly ground surface within a ceramic crucible. The massive support under the crucible is made up of refractory concrete and located between the two heating elements.

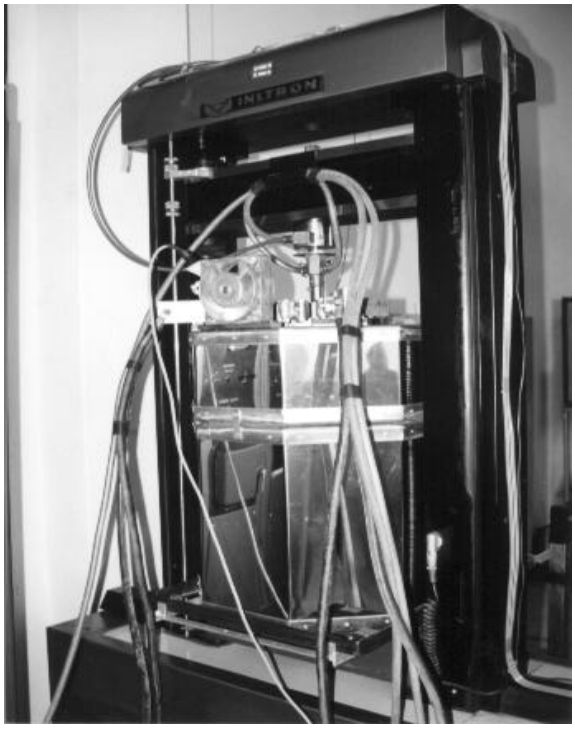

Figure 4. Experimental Apparatus for Hot Deformation Tests

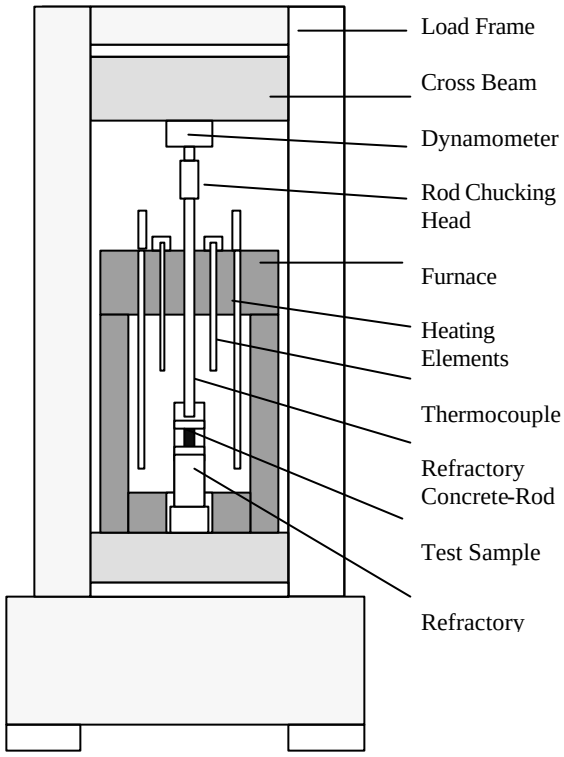

Figure 5. Schematic Diagram for Hot Compression Test Apparatus

A refractory concrete rod with a diameter of 29 mm chucked with the dynamometer can easily slide down the crucible to allow compression as shown in Fig. 6. The design of the set-up enables the steel sample to be accessed from both the top and bottom sides. An inert protective atmosphere is used around the steel sample and is supplied by an inlet in the refractory concrete base.

A cylindrical specimen is used for the hot compression test having an original diameter (D_0) of 15 mm and height (H_0) of 24 mm. The specimen is loaded into the furnace and heated up to the required temperature in the inert protective atmosphere. It is then homogenized in the furnace for 30 min at the pre-set temperature. The tested specimen is compressed by moving the concrete rod down at the pre-set rate. Data on the instantaneous position of the rod and the instantaneous force acting on the rod are recorded by a computer. Once the steel specimen is deformed to one-third of its original height, the downward motion of the rod is stopped and the deformed specimen is then allowed to relax as shown in Fig. 7. The force relaxation with time is also measured and recorded.

Once the relaxation process is completed, the refractory is moved back to its initial position, and the measurement is repeated for a different compression temperature.

Stress And Strain Evaluation

The hot compression tests were conducted between 1369 and 1418 °C which correspond to 0.9 and 0.6 of the solid fraction, respectively. For testing temperatures higher than 1418 °C, the specimens consisting of too much liquid have difficulty to hold together under loading. No attempt has been made to test specimens having the solid fraction lower than 0.6. The solid fraction is defined as weight percentage of solidus component in a mushy state.

The compression velocity (V) is controlled at 8.33×10^{-5} m/s (5 mm/min). For a 24-mm thick specimen, it takes 192 seconds to

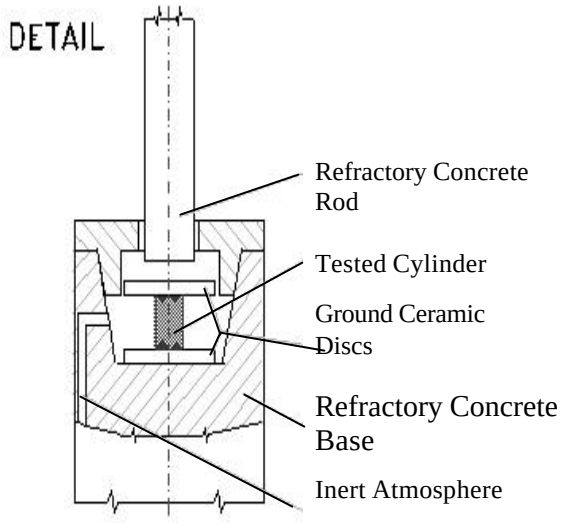

Figure 6. Hot Compression Testing Set

deform to one-third of its original thickness and the corresponding engineering strain rate is 3.47 x 10^{-3} 1/s. The force (P) applied to the test specimen and the height of the specimen (H) were recorded. Then, the engineering stress (S) and engineering strain (e) can be estimated as

$$S = 4P/(\pi D_0^2) \quad (1)$$

and

$$e = (H_0 - H)/H_0 \quad (2)$$

where D_0 and H_0 are the original diameter and height of the specimen, respectively. If the volume of the test specimen is kept constant and the deformation is uniform, the true stress (σ) and true strain (ε) can be respectively calculated as

$$\sigma = (4PH)/(\pi H_0 D_0^2) \quad (3)$$

and

$$\varepsilon = \ln (H/ H_0) \quad (4)$$

The engineering stress-strain results are shown in Fig. 8 for the two different solid-phase contents mentioned. By assuming the deformation being uniform, the corresponding true stress and strain curves are plotted in Fig. 9. The true strain rate can be found as V/H, where V is the compression velocity. Since the deformation is relatively large, by comparing Fig. 8 to Fig. 9, it can be observed that the difference between the true stress-strain curve and engineering stress-strain curve is quite significant. The true stress-strain data should be used for quantifying the "true" flow behavior. Also both figures show that the stress increases as the solid fraction increases.

As shown in Fig. 9, the stress required to deform the specimen greatly increases for true strain less than 18%, then gradually decreases until the true strain has reached 60% before continuing to increase slowly. After releasing the motion, the stress decreases instantly and the material in the mushy state relaxes. It was also observed that at the first few seconds or the initial contact stage, the stress raise in responding to the compression is quite weak and the mushy state material acts more like a liquid or viscous material rather than a solid or elastic material; this is not normally observed in testing fully solidified materials. To further examine this initial viscous behavior, a deformation test at the 0.8 solid fraction was also conducted. Results, also shown in Fig. 9, indeed indicate that the initially weak response is also observed at solid fractions equal to 0.8.

Barrelling

As mentioned earlier, because friction exists between the ceramic discs and specimen, the deformation is not uniform and some barrelling occurs as shown in Fig. 7. The barrelling shape of a cylinder under compressing testing has been quantitatively studied by many investigators. Kulkarni and Kalpakjian (1969), Ettouney and Hardt (1983), Narayanasamy, et. al, (1988), and others have found out that the barrelled shape can be reasonably characterized as the arc of a circle or a circular curvature. In the present study, the barreled shape is defined by an arc of a circle. In this way, the degree of barrelling can be simply quantified by examining the

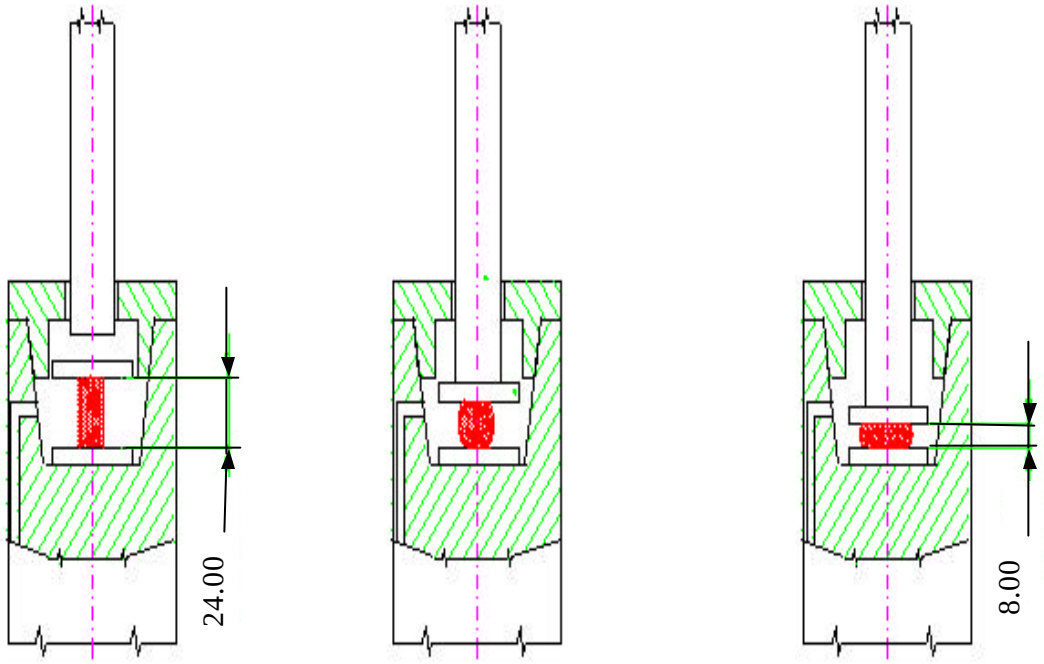

a) Initial position (V = 0) b) Hot upsetting (V =5 mm/min) c) Final position (V = 0)

Figure 7. Hot Compression Testing Procedure

final solidified shape of the specimen.

By trigonometry and from the legends shown in Fig. 10, the radius (R) of the circular curvature AB of the barreled specimen can be found as

$$R = \frac{(D_m - D_e)^2 + H_f^2}{4(D_m - D_e)} \qquad (5)$$

where D_m is the maximum diameter of the barrel, D_e is the end (upper or bottom) cross section diameter of the barrel, and H_f is the final height of the barrel. If the distance between the curvature center and the center of the barreled cylinder is b, the volume (V) of a circular barrel can be found as

$$V = \pi\left\{R^2 H_f - H_f^3/12 + b^2 H_f - b\left[H_f\sqrt{R^2 - H_f^2/4} + 2R^2\sin^{-1}(H_f/2R)\right]\right\} \qquad (6)$$

where b equals $R - D_m/2$ as shown in Fig. 10. If the cylinder specimen is under uniform deformation, R approaches infinite; from the above equation, V becomes $\pi D_f^2 H_f/4$, where D_f is the final diameter of the uniform deformed specimen. Since the volume of the specimen has been assumed constant during the testing, the volume of the barreled specimen in the above equation also equals the original volume, i.e., $V = \pi D_0^2 H_0/4$ or $\pi D_f^2 H_f/4$. As a result, Eq. (6) becomes

$$D_0^2 H_0 - 4\left\{R^2 H_f - H_f^3/12 + b^2 H_f - b\left[H_f\sqrt{R^2 - H_f^2/4} + 2R^2\sin^{-1}(H_f/2R)\right]\right\} = 0 \qquad (7)$$

Mathematically, the deformed portion of the specimen (ΔV) is equal to $\pi H_f (D_f^2 - D_0^2)]/4$ or $\pi D_0^2(H_0 - H_f)/4$; a part of this deformed portion contributes to barrelling and is called the barrelling portion (ΔV_b). If the degree of barrelling (B_d) is defined as the volume ratio of the barrelled portion (ΔV_b) to the total deformed portion (ΔV), one can find that

$$B_d = \Delta V_b/\Delta V = \left[\left(H_0/H_f\right) - \left(D_e/D_0\right)^2\right] / \left[\left(H_0/H_f\right) - 1\right] \qquad (8)$$

Here $\Delta V_b = \pi H_f(D_f^2 - D_e^2)/4$ and $D_f = (H_0 - H_f)^{1/2} D_0$. Since the end-section diameters (D_e) and H_f can be measured from the final shape of the deformed specimen, the parameter B_d can conveniently define the shape of the barrelled specimen by providing the known original parameters, H_0 and D_0. If the specimen is under uniform deformation, the degree of barrelling (B_d) become 0, the edge diameter (D_e) is equal to the final diameter of uniform deformation (D_f). If the specimen is under 100% non-uniform deformation, B_d becomes 1, the diameter of the end section (D_e) is unchanged and equal to the original diameter (D_0).

Normally, the specimen is proportionally deformed and the barrelling parameter B_d can be assumed to be constant during testing. Based on the definition of B_d in Eq. (8), the instantaneous end-section diameter, D_{eh}, at a specific height of the deformed specimen (H) can be found as:

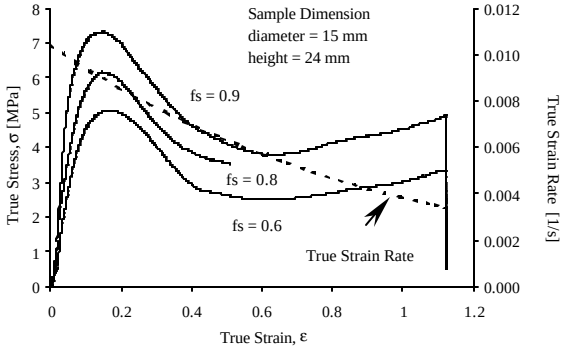

Figure 9. True Stress and True Strain Relationship Without Considering Barrelling

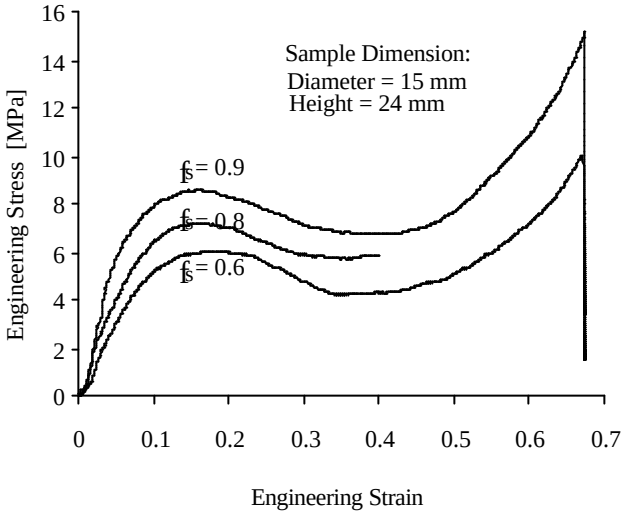

Figure 8. Relationship Between Engineering Stress and Engineering Strain

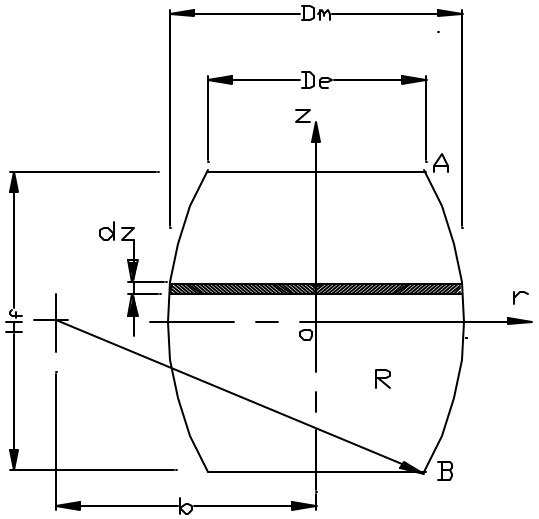

Figure 10. Circularly Barrelled Specimen

$$D_{eh} = \sqrt{\left[(1-B_d)\frac{H_0}{H} + B_d\right]}D_0 \qquad (9)$$

The instantaneous maximum diameter D_{mh} at a specific height of H can be numerically calculated from Eq. (7). It is to be noted the ration of D_{mh} to D_{eh} is called the shape ratio used frequently in compression test studies. Consequently, based on Eq. (5), the instantaneous radius of the barrelling curvature, R_h, can be found as

$$R_h = \frac{(D_{mh} - D_{eh})^2 + H^2}{4(D_{mh} - D_{eh})} \qquad (10)$$

Equivalent Stress and Strain Relationship

If barrelling occurs, the deformation is not uniform; the stress components including shear, radial, and circumferential stresses also exit. The true stress obtained from Eq. (3) should be considered as the mean axial stress only. As a result, the true stress estimation in Eq. (3) should be modified to include the effects of other existing stress components:

$$\sigma_e = C_{mh}\,(4PH)/(\pi H_0 D_0^2) \qquad (11)$$

where σ_e is the equivalent flow stress which includes the effect of all existing stress components; C_{mh} is the correction factor. The correction factor used in Eq. (11) is similar to the correction factor for stresses in the necking region of a uniaxial tensile specimen (Bridgman, 1952). If the shape of the barrelled surface can be characterized by a circular curvature, the correction factor can be found from Ettouney and Hardt, (1983):

$$C_{mh} = \left\{\left[1 - \frac{2R_h}{D_{mh}}\right]\ln\left[1 - \frac{D_{mh}}{2R_h}\right]\right\}^{-1} \qquad (12)$$

Here, the instantaneous maximum diameter, D_{mh}, and the instantaneous radius of the barrelling curvature, R_h, can be found from the procedures presented in the preceding section. Again, if the specimen is uniformly deformed, C_{mh} becomes 1 and R_h approaches infinite.

Based on the original and the final solidified geometries of the tested specimens, the dimensions of D_0, D_e, H_0, and H_f were measured and used to estimate barrelling parameter, B_d. In the present study, the estimated barrelling parameters, B_d, for all specimens tested are around 0.25. It is to be noted that frictional restraint retards the growth of the end cross-section, and part of the new end cross-section is actually formed by folding the sides of the original cylinder onto the platen (end) surface. As a result, the degree of barrelling, B_d, is normally smaller than 0.5.

During testing, the barrelling factor of the specimen has also been assumed to be constant around 0.25. As a result, the instantaneous maximum diameter (D_{mh}), the instantaneous end-section diameter (D_{eh}) and the correction factor (C_{mh}) at a specific deformation stage or strain can be estimated and are plotted in Fig. 11 based on the procedures presented in the preceding section. The values presented in Fig. 11 have been normalized by their value at the strain equal to 0. By providing the information on C_{mh}, the true equivalent stress can then be estimated from Eq. (11) and are depicted in Fig. 12 at the barrelling factor B_d = 0.25. The result shown in the figure should be considered as the true flow stresses and be equivalent to the stress and strain relationship obtained from specimen under uniform deformation.

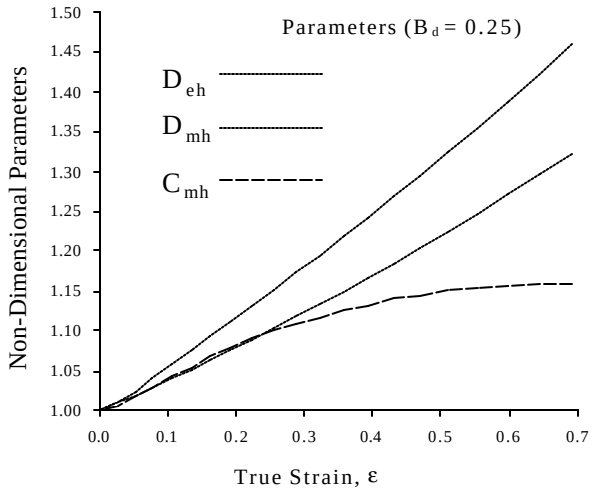

Figure 11. Variations of Barrelling Parameters

The concave shape in the stress-strain curves displayed in Fig. 9 or 12 is not unexpected. The fact that the flow stress increases, then decreases, and increases again as the stain increases has been observed in many studies dealing with relatively low-melting temperature materials at mushy states, including lead-tin alloys by Suery and Flemings (1982) and aluminium alloys by Kiuchi, Sugiyama, and Arai (1979). In fact, the concave shape in the stress-strain curves has also been observed for fully solidified steels at relatively high-temperature deformations; the phenomenon of the stress increase is mainly caused by the effect of strain hardening (Senuma, et al., 1984; Wang and Tseng. 1995). Figure 13 shows the corresponding time history of the loading applied during the hot compression test. Since the loading velocity was held constant, the results in the first 192 seconds are similar to the behaviour shown in Fig. 9 or 12, the relationship of the stress versus strain. The results after 192 seconds show the characteristics of material relaxation and force (stress) reduction. As expected, the stress relaxes exponentially.

Effects of Solid Fraction

The stress-strain curves presented in Fig. 9 or 12 do not exhibit what is known as a sharp yield point which often occurs in iron and steel alloys. Before this point, the stress rises with almost negligible plastic deformation. At this point the material begins to yield. Frequently, the stress at this point is used to represent the strength of the metal considered and called the yield strength. In the present study, the representing strength at the mushy state is selected based on the flow stress at 4% strain. The relationship between the flow stress at 4% strain and the solid fraction for the steel considered is then studied. The peak flow stress and the stress at 10% strain are also selected for comparison.

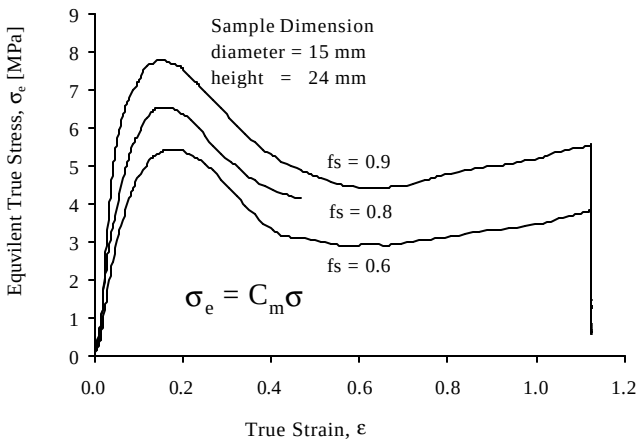

Figure 12. Relationship Between Equivalent True Stress and True Strain

As mentioned earlier, Kiuchi and his associates (1979, 1989) have also used the compression test to study the flow stress at the mushy state and adopted the flow stress at 4% strain as the representing flow stress; they developed the relationship between the representing flow stress and the solid fraction for many metals, including Pb, Al, and Cu alloys and found that the flow stress increases exponentially as the solid fraction increases. Recently, in addition to Kiuchi and his associates' data, Tseng, Chaidilokpattanakul, and Chen (1999) have studied the data obtained by Flemings (1991), Kattamis and Mehrabian (1991), and Dalhe and Arnberg (1993) for the aluminium alloys at mushy states, and found out that all the available data can fit very well by

$$s_f = Ae^{Bf_s} \qquad (13)$$

where σ_f is the representing flow stress; f_s is the solid fraction, and A and B are correlation constants. Based on the results presented in Fig. 12, the equivalent flow stresses at 4% and 10 % strains as well as at the peak are correlated with the solid fraction and depicted in Fig. 14.

Table II Correlation Constants for Equivalent Flow Stress

B_d = 0.25	**A**	**B**	$\mathbf{R^2}$
Peak Stress	2.6550	1.1684	0.966
Stress at 4%Strain	0.6062	2.2350	0.931
Stress at 10%Strain	1.9995	1.4023	0.974

The corresponding correlation constants A and B are listed in Table II. The corresponding correlation coefficients, R, are also estimated. The coefficient always lies between –1 and +1; it is zero when the two variables (σ_f and f_s) selected are totally independent of one another, while it reaches 1 when the two variables correlate perfectly, i.e., no deviation from the correlation of Eq. (13) (Coleman and Steele, 1989). As shown in the table, the square of the correlation coefficient for the three cases considered is higher than 0.93 which means that the data fit very well with the correlation equation.

As shown in Fig. 14, the representing flow stress at 4% strain increases 20% asr the solid fraction dilates from 0.9 to 1.0, while the corresponding flow stresses at 10% strain and at the peak only grow about 10%. As the solid fraction reaches 0, the flow stresses at 4% strain, 10 % strain, the peak, are reduced to 0.61, 2.00, and 2.66 MPa, respectively. The reduction of the flow stress at 4% strain is much larger than those at 10% strain and at the peak. This indicates that the deformation mechanism at 4% strain should be different from those at 10% strain and at the peak. As shown in Fig. 14, at 4% strain, the deformation is somewhat uniform while at 10% strain, the flow stress is close to the peak stress.

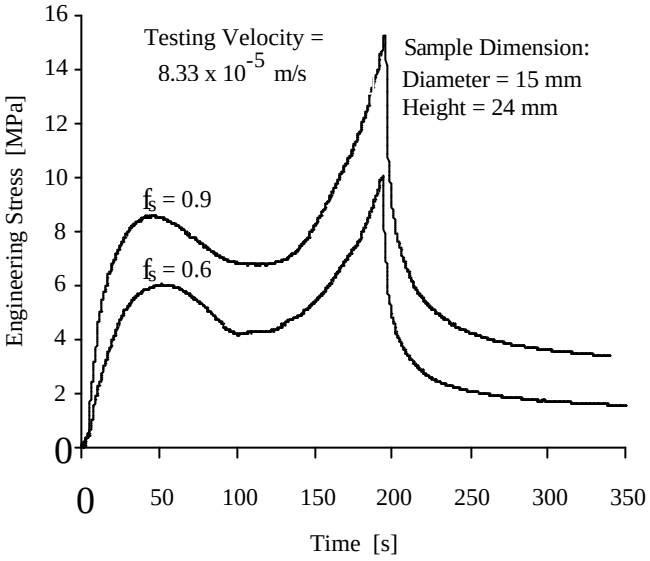

Figure 13. Time History of Compressive Engineering Stress at Two Solid Fractions

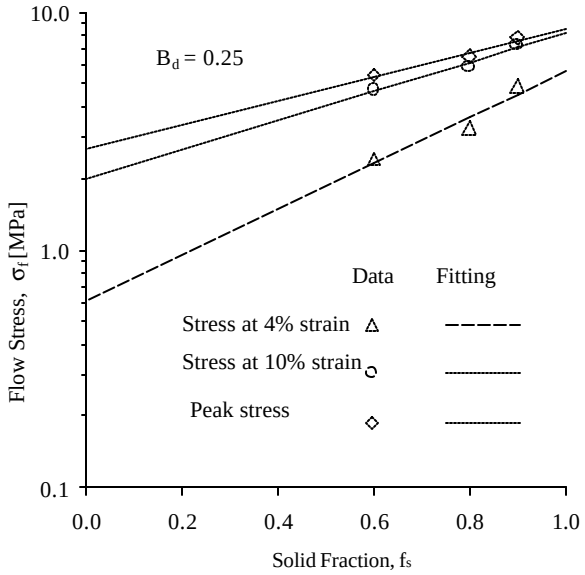

Figure 14. Effects of Solid fraction on Representing Flow Stresses

Based on the explanation by Kiuchi, Sugiyama, and Arai (1979), the deformation at 4% strain is in the region that is still governed by the grain deformation of the solidus component while the deformation at 10% strain or at the peak stress has increasing effect from the liquidus component, which makes the relative slip among grains and the rotation of grain easy, gradually decreasing the amount of grain deformation. Further study is needed to quantify the deformation mechanism, so that the representing flow stress can be appropriately selected. Nevertheless, the present results are consistent with those obtained by Kiuchi, Sugiyama, and Arai (1979) for the case of Al-0.93%Si alloy, in which the solid fraction diminishes from 1.0 to 0.8, the flow stress at 4% strain reduces about 50%. It is should be noted that for the solid fraction decreasing from 1.0 to 0.8, Kiuchi, Sugiyama, and Arai (1979) observed that the flow stress reduction can be larger than 70%, if the alloys have relatively small grain size. Again, further study should be encouraged to investigate the deformation behavior at the mushy state.

Concluding Remarks

The basic deformation behavior of steel in mushy states has been studied. A hot compression tester has been developed to provide the flow stress data of steel at various mushy-states. The tester has specifically designed to accommodate the high temperatures required to melt steels. The temperature of specimens was carefully controlled to correlate the solid phase content.

The mushy states for the solid fraction between 0.6 and 0.9 were evaluated. It has been observed that for the solid fraction less than 0.6, the specimens consisting of too much liquid had difficulty to stably hold together under pressure. The relaxation of steel and stress reduction at mushy states were quantified and discussed.

All results indicate that the flow stresses of steels in mushy states are highly dependent on the solid phase percentage or the solid fraction. Correlations have been developed between the solid fraction and several levels of flow stresses. The predictions from the correlations developed are consistent with those of the correlation developed for other relatively low-melting temperature metals. The correlation developed here can be conveniently used for predicting force or energy required in forming steel parts in mushy states.

Formulas have been developed to quantify the barrelling effects occurring in compression test. The formulas only need the information of the dimension of the original and the final solidified geometries of the tested specimens; since no extra effort is required to obtain this information, the formulation is relatively easy to be adopted. In fact, the formulas are based on the assumption that the degree of barrelling or the barrelling factor is constant during testing. This assumption is consistent with earlier experiment observation and the formulas should be general enough to be applied to all kinds of compression tests. Although the present formulas do not require the information on friction between the test plates and specimen, it is believed that the interface friction and the degree of barrelling are somewhat related. This is similar to the situation that uses the ring compression test to quantify the interface friction coefficient between the die and the cylinder specimen; in estimating the friction, only the dimension information of the original and final geometries of the cylindrical specimens is required (Kalpakjian, 1997). Some further study to find the correlation between the friction coefficient and the barrelling factor should be encouraged.

Since the yield or ultimate strength is difficult to be defined based on the stress and strain curves obtained for the steel in mushy states. In the present study, the flow stresses at three different strains have been selected as the reference strengths of mushy-state steels. However, the characteristics of the correlations between the solid fraction and each flow stress selected are somewhat different. It is believed that the deformation mechanism at different deformation regions should be different. Further study is recommended to quantify the deformation mechanism at different region, so that the representing strength can be appropriately defined. At the time being, however, the deformation behavior at different region should all be studied to provide background information for further study.

Acknowledgements

The authors gratefully acknowledge the support to this research by the US-Czechoslovak Science and Technology Program under Grant No. 94-045 through US National Institute of Standards and Technology, and by the U.S. National Science Foundation under Grant No. DMI-9696062, DMI-9812984 and DMI-0002466.

References

1. Boyer, H. E. and Gall, T. L., ed. (1985), Metals Handbook, Desk Ed., Chapter 28, American Society for Metals, Metal Park, OH.
2. Bridgman, P. W. (1952), Studies in Large Plastic Flow and Fracture, McGraw-Hill, New York, NY.
3. Coleman, H. W. and Steele, W. G. (1989), Experimentation and Uncertainty Analysis for Engineers, John Wiley & Sons, New York, NY.
4. Dahle, A. K. and Arnberg, L. (1996), "The Rheological Properties of Solidifying Aluminum Foundry Alloys", JOM, Vol. 48, No. 3, pp. 34-37.
5. Ettouney, O. and Hardt, O. E. (1983), "A Method for In-Process Failure Prediction in Cold Upset Forging," Paper No. 83-Prod-6, ASME.
6. Flemings, M. C. (1991), "Behavior of Metal Alloys in the Semisolid State," Metallurgical Transactions B, Vol. 22B, pp. 269-293.
7. Kalpakjian, S. (1997), Manufacturing Processes for Engineering Materials, 3rd ed., Addison-Wesley Longman, Menlo Park, NY.
8. Kattamis, T.Z. and Mehrabian, R. (1991), "Rheology of Semisolid Al-4.5%Cu-1.5%Mg alloy", Materials Science and Engineering, Vol. A131, pp. 265-272.
9. Kattamis, T. Z. and Piccone, T. J. (1991), "Rheology of Semisolid Al-4.5%Cu-1.5%Mg Alloy," Materials Science and Engineering, pp., 265-272.
10. Kiuchi, M. (1989), "Metal Forming in Mashy State," in Plasticity and Modern Metal-Forming Technology, ed. by T. Z. Blazynski, Chapter 11, pp. 289-313, Elsevier Applied Science, NY.

11. Kiuchi, M., Sugiyama, S., and Arai, K. (1979), "Study of Metal Forming in the Mashy State 1st Report: Flow Stress and Deformation Behaviour of Alloys in Mashy State," in Proc. 20th Int. Machine Tool Design and Research Conf., pp. 71-78.
12. Kiuchi, M. and Sugizama, S. (1992), "A New Process to Manufacture Semi-Solid Metals," in Proceedings of 2nd Int. Conf.on the Semi-Solid Processing Alloys and Composites, ed. by S. Brown and M.C. Flemings, pp. 47-56.
13. Kulkarni, K. M. and Kalpakjian, S. (1969), "A Study of Barrelling as an Example of Free Deformation," ASME J. Eng. Industry, Vol. 91, pp. 743-754.
14. Kumar, P., Martin, C. L., and Brown, S. (1993), "Shear Rate Thickening Flow Behavior of Semisolid Slurries," Metallurgical Transactions A, Vol. 24A, pp. 1107-1116.
15. Narayanasamy, R., Murthy, R. S. N., Viswanatham, K., and Chary, G. R. (1988), "Prediction of The Barreling of Solid Cylinders Under Uniaxial Compressive Load," J. Mechanical Working Tech., Vol. 16, No. 1, pp. 21-30.
16. Senuma, T., Yada, H., Matsumura, Y., Hamauzu, S., and Nakajima, K. (1984), "Calculation Model of Resistance to Hot Deformation in Consideration of Metallurgical Phenomena in Continuous Hot Deformation Processes," Trans. Iron and Steel Inst. Japan, Vol. 70, No. 19, pp. 78-85.
17. Suery, M. and Flemings, M. C. (1982), "Effect of Strain Rate on Deformation Behavior of Semi-Solid Dendritic Alloys," Metallurgical Transactions A, Vol. 13A, pp. 1809-1819.
18. Tseng, A. A., Chaidilokpattanakul, C. and Chen, J. S-J. (1999), "A Versatile Thermal-Mechanical Model for Twin-Roll Casting," in Manufacturing Science and Engineering-1999, MED-Vol. 10, pp. 57-65, American Society of Mechanical Engineers.
19. Wang, S. R. and Tseng, A. A. (1995), "Macro- and Micro-Modeling of Hot Rolling of Steel Coupled by a Micro-Constitutive Relationship," Materials & Design, Vol. 16, No. 6, pp. 315-336.
20. Worster, M. G. (1997), "Convection in Mushy Layers," Annu. Rev. Fluid Mech., Vol. 29, pp. 91-122